Materials Today: Proceedings xxx (xxxx) xxx

Contents lists available at ScienceDirect

Materials Today: Proceedings

journal homepage: www.elsevier.com/locate/matpr

Effects of physical orientation of dye molecules and molecular orbitals on performance of solid-state dye sensitized solar cells

P.K.D.D.P. Pitigala [a,b,c,*], M.M. Henary [d], A.G.U. Perera [c]

[a] Department of Physics, University of Sri Jayewardenepura, Gangodavila, Sri Lanka
[b] Center for Advance Material Research, University of Sri Jayewardenepura, Sri Lanka
[c] Department of Physics and Astronomy, Georgia State University, Atlanta, GA, United States
[d] Department of Chemistry, Georgia State University, Atlanta, GA, United States

ARTICLE INFO

Article history:
Received 9 March 2019
Received in revised form 6 June 2019
Accepted 10 June 2019
Available online xxxx

Keywords:
Dye solar cells
Cyanine dye
Molecule-orientation
Molecular orbitals
HOMO/LUMO

ABSTRACT

Performance of Dye-sensitized devices depends on the photon absorption and carrier injection properties of the sensitizer (dye). The orientation of the dye molecule affects the photon absorption cross-section, injection efficiency and carrier transport. These effects are studied, using three variants of cyanine dyes in *n*-TiO_2/Dye/*p*-CuSCN heterojunction. The results show correlation of dye-molecule's orientation on the short-circuit-photocurrent (I_{sc}). The open-circuit-voltage (V_{oc}) is also subjective. The orientation of the dye molecule influence the photon-harvesting efficiency and obstruct the hole-conductor penetrating onto the working-electrode. Additionally, Cumulative effects of e-e, e-h, spin-coupling and HOMO/LUMO distribution are identified.

Peer-review under responsibility of the scientific committee of the Advanced Materials for Clean Energy and Health Applications (AMCEHA).

1. Introduction

Studies on dye sensitized solar cells (DSSCs), as a viable low cost solar energy conversion device, were initiated around late 1960s [1]. The first reasonably efficient DSSC was reported by O'Regan and Grätzel in 1991; where use of highly nano-porous anode enabled the enhancement of the efficiency [2]; subsequently, there have been many developments in the field [3,4]. One of the main areas of DSSC research is synthesis of different dyes which have better photon-absorption, carrier transport and chelation properties. In addition to the N3 dye, the black dye and the Z907 are few of the popular and high efficient dyes used in DSSCs [5–7]. These dyes are ruthenium (Ru) based dyes, where carrier transfers in the dye is based on the process of electrons moving from metal to legend. In addition to these metal based dyes, metal-free dyes have also been examined where the charge transfer in the molecule is based on the Donor-π bridge-Acceptor (D-π-A) mechanism. Apart from the low cost, metal-free dyes also have some fundamental advantages over the Ru-based dyes [8]. Furthermore, in addition to use of different single dyes, dye anionic-cationic combinations [9], co-absorbents [10–13], organized aggregated dye layers [14,15] and natural dyes [16–18] have been used in DSSCs to improve their photon-to-current conversation efficiencies. Many other innovative variations of dyes and electrode materials have also been studied in order to understand the device properties and develop a high efficient dye sensitized devices for solar energy conversion [19–21].

The light harvesting efficiency (LHE) of a solar cell is one of the factors determines its efficiency. If the Γ represents the number of sensitizer molecules in a square centimeter in the device and the σ is the effective light absorption cross-section area of the dye, the LHE, as a function of wavelength can be given by,

$$LHE(\lambda) = 1 - 10^{-\Gamma\sigma(\lambda)} \quad (1)$$

The absorption of photons by the dye molecule depends on the orientations of the dye molecules anchored onto the semiconductor surface (the light absorption cross-section area) hence contribute to the LHE of the device. The Dyes anchoring on to TiO_2 surfaces, will have different orientations depending on the interactive forces between the dye molecule and the TiO_2 surface [22] and the positions of the bonding legends in the dye molecule [23]. Additionally, the orientation of the dye can influence the charge transfer energies of the molecule [24] hence effecting the performances of a dye sensitized devices.

* Corresponding author at: Department of Physics, University of Sri Jayewardenepura, Gangodavila, Sri Lanka.
E-mail address: dpitigala@sjp.ac.lk (P.K.D.D.P. Pitigala).

https://doi.org/10.1016/j.matpr.2019.06.189
2214-7853/
Peer-review under responsibility of the scientific committee of the Advanced Materials for Clean Energy and Health Applications (AMCEHA).

2. Materials and procedure

The three cationic pentamethine cyanine dyes, named T-49, T-50, and T-55 (structural formulae shown in Fig. 1), were synthesized based on our previous published procedures [15,25–33]. In brief, the final compounds were synthesized from commercially obtained unsubstituted phenyl hydrazines (CAS: 100–63-0). The hydrazines were dissolved in acetic acid (50 mL) and 1 M eq. of 3-methyl-2-butanone (CAS: 563-80-4) and heated under reflux for 72 h. The resulting reaction mixture was worked up using sodium bicarbonate to neutralize the acid and then extracted and separated with dichloromethane. The organic layer was dried using $MgSO_4$ and evaporated under reduced pressure. The resulting oil was heated at reflux with 1.1 M eq. of 3-bromopropionic acid (CAS: 590-92-1) and acetonitrile for 24 h. The reaction mixture was evaporated and the product was crystallized from dichloromethane and diethyl ether. The brown crystals were dried under vacuum for 24 h before proceeding to the final step. The indolenine salts were dissolved in acetic anhydride with 0.5 M eq. of malonadehyde bisphenyl linker and 5.1 M eq. of sodium acetate. The reaction mixture was heated under reflux for 30 min for the completion of the reaction. The reaction mixture was evaporated under vacuum to give a solid residue and then purified using solvent transfer crystallization using DCM and diethyl ether. The pure crystals were characterized using ^{1}H NMR, ^{13}C NMR and Mass Spectrometry [28,29,31–33].

TiO_2 films were prepared on fluorine-doped-conducting tin oxide (FTO) glass plates (1.0×1.5 cm^2) by hydrolyzing titanium-isopropoxide in 75% propan-2-ol, and acetic acid (20% in volume) mixture of 1:3:1 ratio in volume. The hydrolyzed product is mixed with Degussa P25 TiO_2 powder and this viscous slurry was spread over (1×1 cm^2 area) the FTO plate preheated to 120 °C. After spreading the slurry the plate was left at 120 °C for about 5 mins, then the loose crust of TiO_2 particles not adhered to the FTO surface are blown off and the plate is heated in an oven at 425 °C for 10 mins. Repeated the process till the TiO_2 film is grown to a desired thickness (~10 μm).

Each of the above cationic cyanine dye (~5 mg) were dissolved in 200 proof ethanol (5 mL) and these dyes were coated over the TiO_2 film by the following procedure. TiO_2 film is thoroughly cleaned with alkaline 50% propan-2-ol followed by water and 99% propan-2-ol and plate dried at 120 °C. Dried plate is positioned vertically in a small glass vial and the films are soaked in the dye solution for ~15 h. Dye film is dried in air at ambient temperature and p-CuSCN deposited over the dye coating from a saturated CuSCN solution in n-propyl sulfide [34]. The back contact is formed by pressing a FTO glass plate to secure the contact and a thin graphite layer was used over the CuSCN surface to improve the back contact. The IV characteristics of the cells were recorded using a calibrated halogen lamp and a KEITHELY 2400 source meter, and the photocurrent action spectra was measured using a SP-DK480 monochromator and a SR-850 lock-in amplifier set-up calibrated with a standard silicon photodiode. The absorption spectra were obtained using Ocean Optics USB2000 UV–VIS spectrometer. The built in functions of the Chemdraw® (Chem3D Pro 12.0) software was used to evaluate following parameters, the HOMO-LUMO, the MM2 Minimization of the molecules and to calculate the solvent accessible surfaces of the molecules.

3. Results and discussion

The current-voltage (IV) characteristics of the devices sensitized with the three dyes, T-49, T-50 and T-55, are shown in the Fig. 2. The chemical structures of the dyes shows the same base structure apart from the halogen atom in the meso-carbon of the methine chain, for example: T-50 has a bromine (Br) atom and T-55 has a chlorine (Cl), while the T-49 does not have a halogen atom. These differences in the dye structures had effected on the open-circuit voltage (V_{oc}) and the short circuit current (I_{sc}) of the device. In the big picture, the halogen atom has clearly affected the I_{sc}. The I_{sc} is increased approximately by a factor of two in the device with T-50, which have the Br atom, compared to the T-49 that does not have a halogen atom. Furthermore, the T-55, with the Cl atom, has a higher I_{sc} compared to T-49, but it is lower than that of with T-50. The V_{oc} of T-55 was the highest and even though T-50 and T-49 have their V_{oc} very close, statistically T-50 has the lowest $V_{oc.}$ of all.

The absorption spectra of the three dyes (measured in ethanol), have shown identical thresholds within a range of experimental error and a similar spectral profile with a small deviations from each other as can be seen in the Fig. 3. In contrast, the dyes T-49, T-50, and T-55 have extinction coefficients of 60700, 32200, and 24500 $M^{-1}cm^{-1}$ respectively in ethanol and the area of each molecule is ~53.2, ~53.2 and ~54.7 nm^2 respectively. The dye loading calculations estimates approximately 1.9×10^{14}, 1.8×10^{14} and 1.8×10^{14} dye molecules of T-49, T-50, and T-55 respectively anchored on the TiO_2 films. Therefore, according to Eq. (1), the LHE should be same for all three dyes, as the molecular areas and the number of molecules of the three dyes are respectively similar, so should the photocurrent since I_{sc} is directly related to

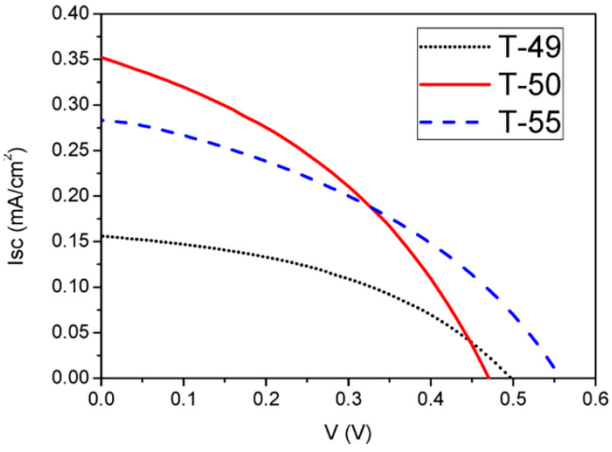

Fig. 2. The I-V characteristics of devices sensitized by different dyes T-49, T-50 and T-55 in the device configuration TiO2/Dye/CuSCN.

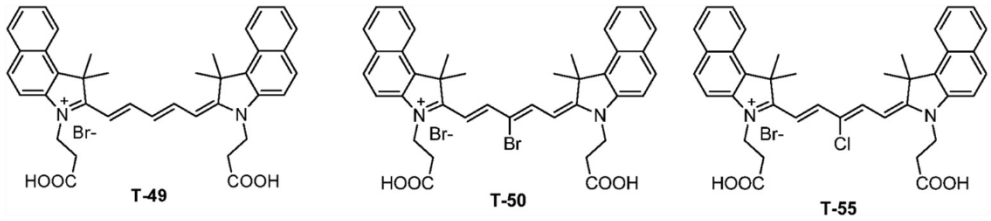

Fig. 1. Chemical structures of the three cationic cyanine dyes T49, T-50 and T-55.

Please cite this article as: P. K. D. D. P. Pitigala, M. M. Henary and A. G. U. Perera, Effects of physical orientation of dye molecules and molecular orbitals on performance of solid-state dye sensitized solar cells, Materials Today: Proceedings, https://doi.org/10.1016/j.matpr.2019.06.189

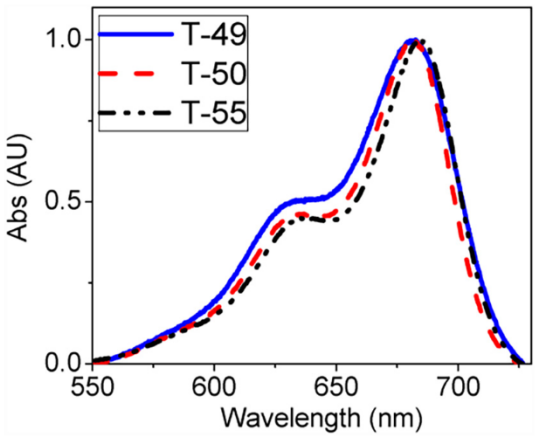

Fig. 3. The normalized absorption spectra for the T-49, T-50 and T-55 in 200 proof ethanol. The three dyes show similar thresholds and a spectral profile. The peak position of T-55 was red shifted compared to the other two dyes. (For interpretation of the references to color in this figure legend, the reader is referred to the web version of this article.)

the LHE. But, the experimental results have deviated from this theoretical prediction (I_{sc} of the devices decreased as T-50 > T-55 > T-49). The reason for this deviation can be a result of the dye chelation effecting the carrier injection and orientation of the dye on the TiO_2 film affecting the light absorption area.

Dye molecules with carboxylic ligands are known to anchor on to the TiO_2 surface *via* those COOH groups, by forming bidentate or mono-dentate bonding. Since the three dyes under examination have a couple of COOH groups, depending on their orientation, the dyes can anchor by either one or both the carboxylic groups. The MM2 dynamics and MM2 minimization calculations available on ChemDraw® were used to identify the dye molecules' orientation prior to chelate with TiO_2. The Fig. 4 shows the schematic of these free dye structures' orientation in a view approximately normal and parallel to the plane of the dye structures. The MM2 calculations indicated that the two carboxylic groups rotate and orient to be in the Trans to each other. Here in the three dyes, the COOH group probing into the pyrrolidinium *N* atom is oriented in a perpendicular plane to the plane of the dye molecule; while the COOH group attached to the immonium *N* site in the benz[e] indoleninium moiety is in the same plane. Hence the probability of the dyes anchoring with both the COOH groups will be rare in a probability. This was further confirmed by the energy calculated via the MM2 minimization, that shows it is energy vice favorable for the molecules to attached onto TiO_2 via a single COOH group not by both. Additionally, except for the T-55, the other two dyes showed the favorable energy when attached with the COOH group probing in to the pyrrolidinium *N* atom instead of *N* atom in the benz[e] indoleninium moiety Therefore, in the devices the T-55, will be attached to the TiO_2 by bonding at the *N* atom in the benz[e] indoleninium moiety and the T-49 and T-50 are attached with the TiO_2 by the pyrrolidinium *N* atom.

The HOMO-LUMO molecular orbital (MO) distribution on each dye molecule, T-49, T-50 and T-55, were calculated using the Extended Huckel function available in ChemDraw®. As can be seen in the Fig. 5, when a TiO_2 mesh is attached to the dye molecule, the LUMO and HOMO states in each dye molecule are spread along the two benz[e] indoleninium moieties in the molecule. Furthermore, the number of MOs is also different in each dye molecule. The T-49 has a very low number of HOMOs and LUMOs, and the highest number of MOs is visible on the T-50 molecule. This gives a direct correlation between the number of MOs and the I_{sc}. Moreover, on both the T-49 and the T-55, majority of the LUMO states were shifted away from the COOH group anchored on to the TiO_2 surface, while the T-50 have more evenly distributed LUMO states along the molecule with few on the center chain and also nearby the anchoring COOH group compare to the other two dyes. The directional positioning of these HOMOs and LUMOs are important as the charge transfer mechanism in these dyes will be based on the D-π-A mechanism. The COOH group is expected to act as the acceptor (A), while the donor (D) is the benz[e] indoleninium moiety; hence, there should be LOMOs on or neighboring the bonding COOH ligand in order to facilitate the electron transfer on to the semiconductor material. In contrast, as can be seen in the Fig. 5, even though HOMOs exist on the benz[e] indoleninium moiety, except for the T-50, the other two dyes do not have the LUMO states on the COOH group anchored onto the TiO_2. This clarifies the low I_{sc} in T-49 and T-55 compared to the T-50. Additionally, few other correlations described below were also observed during this study.

The correlation between the distance to the closest LUMO from the anchoring ligand, and the short-circuit photocurrent: The T-50 have shortest distance from the LUMO states to the dye anchoring location onto the TiO_2 surface of all three dyes, including a LUMO on the COOH ligand. The T-55 has the next nearest LUMO site to the anchoring point, while the T-49 has the longest distance. The closest LUMO state in T-49 is approximately two times the length of C = C further than that of T-55. This can be the result of having a higher I_{sc} in the device sensitized with T-55 compared to that with T-49. This confirms a correlation, between the distances of the closest LUMO position with respect to the anchoring point, on the I_{sc} in the device. Furthermore, the T-49 has one of its HOMO closer to the TiO_2 surface, which also can form a reductive quenching pathway resulted in reducing the I_{sc}. For the moment there is

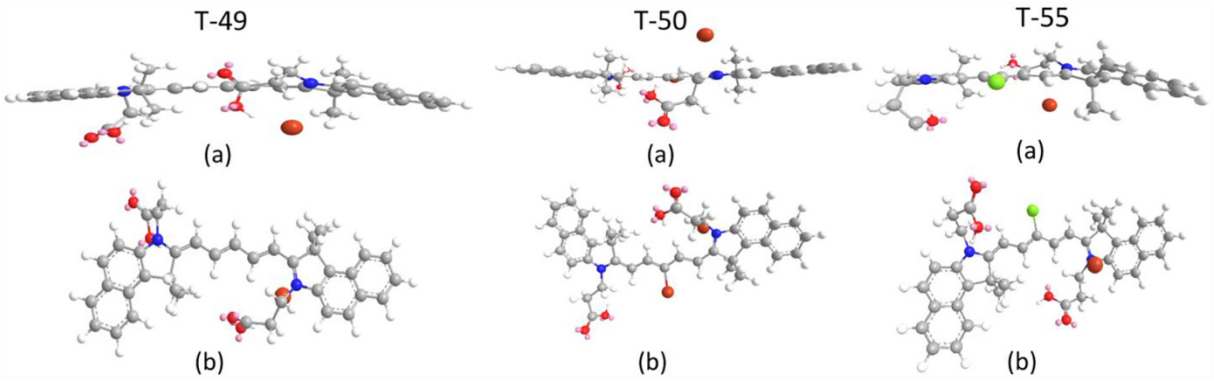

Fig. 4. A schematic of the dye molecules' orientation in a view (a) parallel and (b) normal to the plane of dye surface.

Please cite this article as: P. K. D. D. P. Pitigala, M. M. Henary and A. G. U. Perera, Effects of physical orientation of dye molecules and molecular orbitals on performance of solid-state dye sensitized solar cells, Materials Today: Proceedings, https://doi.org/10.1016/j.matpr.2019.06.189

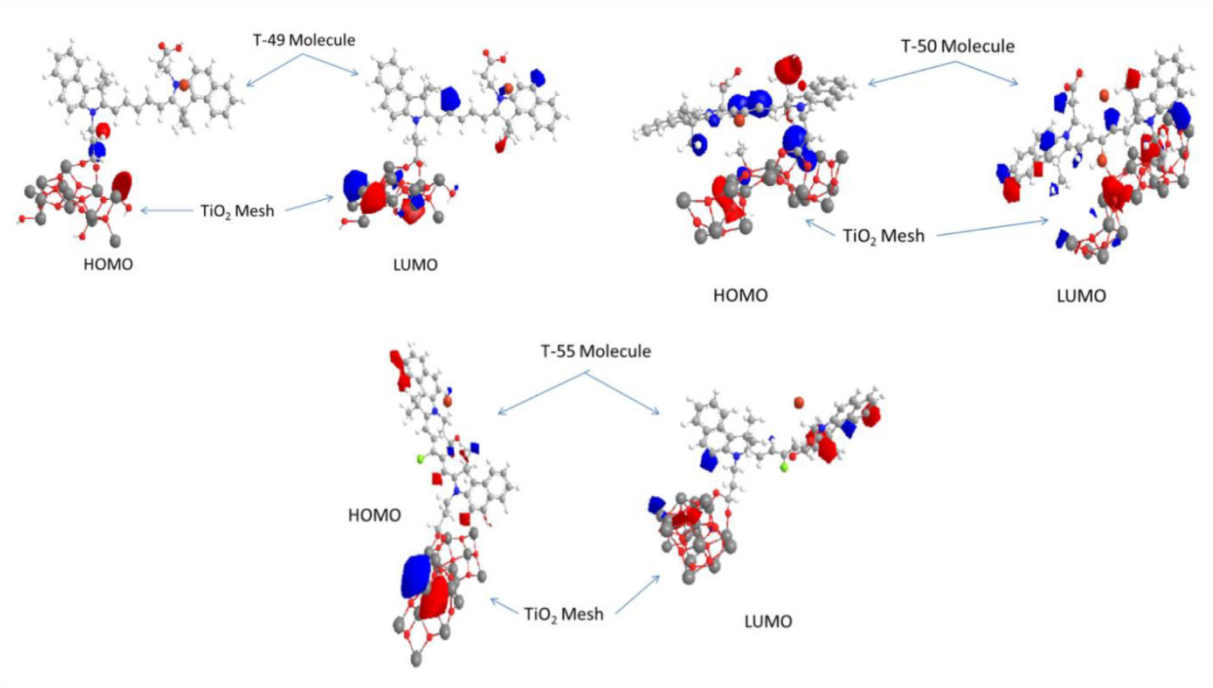

Fig. 5. The HOMO and LUMO positions of the dyes (T-49, T-50 and T-55) after anchoring on to the TiO_2 mesh. In the figure, for T-50 and T-55, the molecule is rotated between the HOMO and LUMO images for better view.

no clear understanding of which of the above two have the greater effect, but the comparatively low I_{sc} in T-49 is a result of the combination of both of the above effects.

The variation in the orientation of the dye structure, with respect to the TiO_2 surface: As can be seen in Fig. 5, the T-49 stands near normal to the TiO_2 surface; the T-50 is laid parallel and wrapped or cuddle onto the TiO_2 surface and the T-55 is in an intermediate orientation with partially curved away from the TiO_2 surface. This variations in the dye orientations will vary the effective light absorption area (σ) in the dye and the photon absorption will be effected; hence change the LHE given by Eq. (1). Therefore, another reason for the variation of the I_{sc} in the three devices is this dye orientation. Even though there is no direct proportionality between effective light abortion area and the I_{sc} can be seen in the results (due to the other effects described in this paper), the results in Fig. 2 shows a clear correlation, where the I_{sc} is increasing with the orientation changing from the perpendicular (or near normal) to a parallel, increasing the effective photon abortion area of the dyes, from T-49 to T-55 and to T-50 respectively.

As can be seen in the Fig. 6, the solvent accessible surface of each dye-TiO_2 configuration calculated by the ChemDraw® inbuilt function shows, the T-50 is been cuddled with the TiO_2 without any open space between them there is no space between the dye molecule and the TiO_2 surface. This will prevent the hole-conducting material (p-CuSCN in this study) from penetrating on to the TiO_2 surface. While in the cases of T-49 and T-55 there is some open space between the dye and the TiO_2 surface. Therefore, these orientations can restrict the penetration of the hole-conductor further into the device and spreading onto the TiO_2 surface. As a result of restricting the p-CuSCN penetration onto the TiO_2 surface, the T-50 has avoided or reduced the possible reductive quenching pathways fromTiO_2 to CuSCN, resulting a high I_{sc}. For the other two dyes, the open space between the dye and the TiO_2 allowed the p-CuSCN to penetrate onto the TiO_2 surface. Where, it created reductive quenching pathways resulted in reducing the I_{sc}.

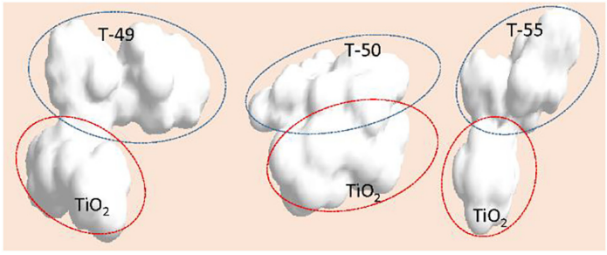

Fig. 6. The solvent accessible surface calculated for each dye-TiO_2 configuration. The lump in the bottom of each cloud like formation is the TiO_2 mesh and the lump on the top is the dye molecule. T-49 and T-55 have space (a gap) between these two lumps, which implies the p-CuSCN can penetrate on to the TiO_2 surface, whilst T-50 has covered (wrapped or cuddled) the TiO_2 surface closely avoiding p-CuSCN penetration on to the TiO_2 surface.

The V_{oc} is also an important parameter in the DSSCs. In general, the V_{oc} is defined by the difference between the conduction band of n-TiO_2 and the valence band level of the hole-conductor. Never the less, we have observed a variant in the V_{oc} in the three devices under study, with the device sensitized by T-50 have the lowest V_{oc} while T-55 have the highest V_{oc}, the effect on V_{oc} with respect to the dye orientation did not show a clear relation in our study. But we can point out few partial relationships we have extracted through our study.

There are few factors that can be assumed to have affected the V_{oc}. One of them is the reductive quenching paths, this explains the higher V_{oc} in T-55 compared to T-49, where T-49 with the perpendicular orientation can create more reductive quenching paths compared to the T-55, because of the higher accessibility of the CuSCN (hole-conductor) on to the TiO_2 film (photo-anode/electron conductor). When the hole-conductor is in contact with the electron conductor Fermi levels get altered in the device, therefore reduces the V_{oc}. In contrast, the T-50, providing the least possibility of penetration and contact between the two materials

Please cite this article as: P. K. D. D. P. Pitigala, M. M. Henary and A. G. U. Perera, Effects of physical orientation of dye molecules and molecular orbitals on performance of solid-state dye sensitized solar cells, Materials Today: Proceedings, https://doi.org/10.1016/j.matpr.2019.06.189

should have the highest V_{oc}, but does not follow with this inference. This implies there may be other factors too involved in the determination of the V_{oc}.

A comparison of V_{oc} between the T-55 and T-50 shows another partial relationship with the LUMO (HOMO) state density in the dye molecule of the dye. Where T-50 with large number of MO states have a low voltage compared to the T-55 with lesser number of MOs. Again the T-49 with the least MOs does not agree with this pattern. Which implies the other factors or combination of orientation and MOs might weigh-in when determining the V_{oc} of the device. The rate of carrier accumulation on these semiconductor materials Burstein-Moss effect; hence alter the effective energy difference between the HOMO LUMO levels in the heterojunctin devices [35], Therefore, it is possible to produce a different V_{oc} for different dyes. The device with T-50, producing more carriers, can have higher e-e, e-h and spin coupling effects compared to T-55 and T-49 with fewer carriers resulting in a lower V_{oc} with it. In this content T-49 should have the highest V_{oc} whilst the reductive quenching paths and the HOMO position near TiO_2 film deviated it to be lower than that of T-55.

The third partial relationship affecting the V_{oc} is associated with the positioning of the HOMO levels and the dye molecule bonding on to the hole conducting material. Our results show a tendency of producing a high V_{oc} when a HOMO state is at the furthest end of the dye molecule as in T-55(at far end of the benz[e] indoleninium moiety) and low V_{oc} if it is closer to the electron conductor (TiO_2) as in T-49 (at near end of the benz[e] indoleninium moiety). Going through some literature [36,37] and analyzing those results, they have also revealed a similar tendency in V_{oc} where the highest V_{oc} was observed in the dye molecule where a HOMO state was located at the furthest end from the TiO_2. Again the T-50 diverted from this pattern. There is a major difference between the T-50 and the other two dyes. In T-50 the furthest HOMO level is on a methyl group in the (at near end of) the benz[e] indoleninium moiety (see Fig. 5). Furthermore, even though the distance to this HOMO state is furthest along the dye molecule, if considered the displacement to this HOMO position from the TiO_2 surface the T-50 holds the lowest displacement compare to the other two dyes. This is one of the possibilities but further studies are needed to confirm these conclusions.

As it can be observed, variation in the V_{oc} in the DSSC can be resulted by conjugation of all above effects. Further studies are required to untangle the effects and to enhance the understanding of extent these effects on a given DSSC.

4. Conclusion

The MM2 calculation shows that the three dyes are creating three different angles with respect to the TiO_2 surface, which results in varying the photon absorption and hence the light harvesting efficiency of the device. Additionally, as can be seen from the solvent accessible surface calculations the dye orientation can prevent the hole conductor from reaching onto the photo anode; hence suppress recombination at the photo anode surface. This ensures a direct effect on the photocurrent and an indirectly effect on the photovoltage of the device. Furthermore, the dye molecules orientation had provoked the HOMO and LUMO energy distribution and the study data clearly shows a relation between these molecular orbital densities and the photocurrent in the device. Additionally, a partial relationship in orientation and HOMO/LUMO state positions on the photocurrent and the photovoltage were also uncovered. Additional studies are required to further enhance the understanding of effects on Voc of the DSSC due to HOMO/LUMO state orientation.

Acknowledgements

This work is partially supported by the US National Science Foundation Grant NSF ECCS 1232184 and the Research grant # ASP/01/RE/SCI/2018/26 awarded by the research council of the University of Sri Jayewardenepura. M.H. thanks the NIH (Grant Nos. R01-EB022230), the Atlanta Clinical & Translational Science Institute for the Healthcare Innovation Program Grant, the Georgia Research Alliance for the Ventures Phase 1 Grant for the support.

References

[1] H. Gerischer, M.E. Michel-Beyerle, F. Rebentrost, H. Tributsch, Sensitization of charge injection into semiconductors with large band gap, Electrochimica Acta 13 (1968) 1509–1515.
[2] B. O'Regan, M. Gratzel, A low-cost, high-efficiency solar cell based on dye-sensitized colloidal TiO2 films, Nature 353 (1991) 737–740.
[3] M. Grätzel, Dye-sensitized solid-state heterojunction solar cells, MRS Bullet. 30 (2005) 23–27.
[4] T. Prakash, Review on nanostructured semiconductors for dye sensitized solar cells, Electr. Mater. Lett. 8 (2012) 231–243.
[5] P. Wang, S.M. Zakeeruddin, I. Exnar, M. Gratzel, High efficiency dye-sensitized nanocrystalline solar cells based on ionic liquid polymer gel electrolyte, Chem. Commun. (2002) 2972–2973.
[6] M.K. Nazeeruddin, P. Péchy, T. Renouard, S.M. Zakeeruddin, R. Humphry-Baker, P. Comte, P. Liska, L. Cevey, E. Costa, V. Shklover, L. Spiccia, G.B. Deacon, C.A. Bignozzi, M. Grätzel, Engineering of efficient panchromatic sensitizers for nanocrystalline TiO2-based solar cells, J. Am. Chem. Soc. 123 (2001) 1613–1624.
[7] M.K. Nazeeruddin, A. Kay, I. Rodicio, R. Humphry-Baker, E. Mueller, P. Liska, N. Vlachopoulos, M. Graetzel, Conversion of light to electricity by cis-X2bis(2,2'-bipyridyl-4,4'-dicarboxylate)ruthenium(II) charge-transfer sensitizers (X = Cl-, Br-, I-, CN-, and SCN-) on nanocrystalline titanium dioxide electrodes, J. Am. Chem. Soc. 115 (1993) 6382–6390.
[8] A. Hagfeldt, G. Boschloo, L. Sun, L. Kloo, H. Pettersson, Dye-sensitized solar cells, Chem. Rev. 110 (2010) 6595–6663.
[9] P.K.D.D.P. Pitigala, M.K.I. Seneviratne, V.P.S. Perera, K. Tennakone, Sensitization of nanostructured TiO2 by electrostatic coupling of ionic dyes to ionic absorbates, Langmuir 20 (2004) 5100–5103.
[10] M.K.I. Senevirathna, P.K.D.D.P. Pitigala, K. Tennakone, Chromopore-linked conducting polymers attached to semiconductor surfaces: a strategy for development of dye-sensitized solar cells, J. Phys. Chem. B 109 (2005) 16030–16033.
[11] M.K.I. Senevirathna, P.K.D.D.P. Pitigala, V.P.S. Perera, K. Tennakone, Molecular rectification: application in dye-sensitized solar cells, Langmuir 21 (2005) 2997–3001.
[12] J.H. Yum, S.J. Moon, R. Humphry-Baker, P. Walter, T. Geiger, F. Nüesch, M. Grätzel, M.d.K. Nazeeruddin, Effect of coadsorbent on the photovoltaic performance of squaraine sensitized nanocrystalline solar cells, Nanotechnology 19 (2008) 424005.
[13] B.L. Watson, T.A. Moore, A.L. Moore, D. Gust, Synthesis of a novel building block for the preparation of multi-chromophoric sensitizers for panchromatic dye-sensitized solar cells, Dyes Pigments 136 (2017) 893–897.
[14] K. Tennakone, P.K.D.D.P. Pitigala, A.G.U. Perera, Exciton transport and electron mobility of organized aggregates of cationic dye thiocyanates, RSC Adv. 3 (2013) 2770–2775.
[15] P.K.D. Duleepa Pitigala, M.M. Henary, E.A. Owens, A.G. UnilPerera, K. Tennakone, Excitonic photovoltaic effect in a cyanine dye molecular assembly electronically coupled to n- and p-type semiconductors, J. Photochem. Photobiol. A: Chem. 325 (2016) 39–44.
[16] H. Hug, M. Bader, P. Mair, T. Glatzel, Biophotovoltaics: natural pigments in dye-sensitized solar cells, Appl. Energy 115 (2014) 216–225.
[17] P.M. Sirimanne, M.K.I. Senevirathna, E.V.A. Premalal, P.K.D.D.P. Pitigala, V. Sivakumar, K. Tennakone, Utilization of natural pigment extracted from pomegranate fruits as sensitizer in solid-state solar cells, J. Photochem. Photobiol. A: Chem. 177 (2006) 324–327.
[18] T.S. Senthil, N. Muthukumarasamy, D. Velauthapillai, S. Agilan, M. Thambidurai, R. Balasundaraprabhu, Natural dye (cyanidin 3-O-glucoside) sensitized nanocrystalline TiO2 solar cell fabricated using liquid electrolyte/quasi-solid-state polymer electrolyte, Renew. Energy 36 (2011) 2484–2488.
[19] M.Y. Song, K.N. Chaudhari, J. Park, D.-S. Yang, J.H. Kim, M.-S. Kim, K. Lim, J. Ko, J.-S. Yu, High efficient Pt counter electrode prepared by homogeneous deposition method for dye-sensitized solar cell, Appl. Energy 100 (2012) 132–137.
[20] J. Gong, K. Sumathy, J. Liang, Polymer electrolyte based on polyethylene glycol for quasi-solid state dye sensitized solar cells, Renew. Energy 39 (2012) 419–423.
[21] F. Rizzi, N.J. van Eck, M. Frey, The production of scientific knowledge on renewable energies: worldwide trends, dynamics and challenges and implications for management, Renew. Energy 62 (2014) 657–671.

Please cite this article as: P. K. D. D. P. Pitigala, M. M. Henary and A. G. U. Perera, Effects of physical orientation of dye molecules and molecular orbitals on performance of solid-state dye sensitized solar cells, Materials Today: Proceedings, https://doi.org/10.1016/j.matpr.2019.06.189

[22] J. McCree-Grey, J.M. Cole, P.J. Evans, Preferred molecular orientation of coumarin 343 on TiO_2 surfaces: application to dye-sensitized solar cells, ACS Appl. Mater. Interfaces 7 (2015) 16404–16409.
[23] Y. Ooyama, Y. Shimada, S. Inoue, T. Nagano, Y. Fujikawa, K. Komaguchi, I. Imae, Y. Harima, New molecular design of donor-[small pi]-acceptor dyes for dye-sensitized solar cells: control of molecular orientation and arrangement on TiO2 surface, New J. Chem. 35 (2011) 111–118.
[24] A. Ojala, A. Petersen, A. Fuchs, R. Lovrincic, C. Pölking, J. Trollmann, J. Hwang, C. Lennartz, H. Reichelt, H.W. Höffken, A. Pucci, P. Erk, T. Kirchartz, F. Würthner, Merocyanine/C60 planar heterojunction solar cells: effect of dye orientation on exciton dissociation and solar cell performance, Adv. Funct. Mater. 22 (2012) 86–96.
[25] E.A. Owens, M. Henary, G. El Fakhri, H.S. Choi, Tissue-specific near-infrared fluorescence imaging, Acc. Chem. Res. 49 (2016) 1731–1740.
[26] E.A. Owens, N. Bruschi, J.G. Tawney, M. Henary, A microwave-assisted and environmentally benign approach to the synthesis of near-infrared fluorescent pentamethine cyanine dyes, Dyes Pigments 113 (2015) 27–37.
[27] C.T. Mapp, E.A. Owens, M. Henary, K.B. Grant, Oxidative cleavage of DNA by pentamethine carbocyanine dyes irradiated with long-wavelength visible light, Bioorg. Med. Chem. Lett. 24 (2014) 214–219.
[28] G. Beckford, E. Owens, M. Henary, G. Patonay, The solvatochromic effects of side chain substitution on the binding interaction of novel tricarbocyanine dyes with human serum albumin, Talanta 92 (2012) 45–52.
[29] G. Chapman, M. Henary, G. Patonay, The effect of varying short-chain alkyl substitution on the molar absorptivity and quantum yield of cyanine dyes, Anal. Chem. Insights 6 (2011) 29–36.
[30] K. Soon Hee, P. Gwangli, H. Hoon, L. Jeong Heon, A. Yoshitomo, C. Jungmun, H. H. Gloria, A.O. Eric, H. Maged, C. Hak Soo, Near-infrared lipophilic fluorophores for tracing tissue growth, Biomed. Mater. 8 (2013) 014110.
[31] M. Mojzych, M. Henary, Synthesis of Polymethine Dyes, in: L. Strekowski (Ed.), Topics in Heterocyclic Chemistry, Springer-Verlag, Berlin Heidelberg, 2008, pp. 1–9.
[32] R. Nanjunda, E.A. Owens, L. Mickelson, S. Alyabyev, N. Kilpatrick, S. Wang, M. Henary, W.D. Wilson, Halogenated pentamethine cyanine dyes exhibiting high fidelity for G-quadruplex DNA, Bioorg. Med. Chem. 20 (2012) 7002–7011.
[33] A.O. Eric, H. Hoon, K. Soon Hee, L. Jeong Heon, P. GwangLi, A. Yoshitomo, C. Jungmun, H.H. Gloria, A. Sergey, L. Sang Jin, K. Gilson, H. Maged, C. Hak Soo, Highly charged cyanine fluorophores for trafficking scaffold degradation, Biomed. Mater. 8 (2013) 014109.
[34] K. Tennakone, P. Abeysooriya, M. Kahanda, C. Kasige, P. Kaviranta, R.H. Wijenayake, Dye sensitization of cuprous thiocyanate photocathode in aqueous thiocyanate, J. Electrochem. Soc. 131 (1984) 1574–1577.
[35] P.K.D.D.P. Pitigala, Y.F. Lao, A.G.U. Perera, Effects of incident photon intensity on the response threshold of p-doped AlxGa1-xAs/GaAs superlattice devices, Infrared Phys. Tech. 64 (2014) 193–197.
[36] D.P. Hagberg, T. Marinado, K.M. Karlsson, K. Nonomura, P. Qin, G. Boschloo, T. Brinck, A. Hagfeldt, L. Sun, Tuning the HOMO and LUMO energy levels of organic chromophores for dye sensitized solar cells, J. Org. Chem. 72 (2007) 9550–9556.
[37] T. Marinado, D.P. Hagberg, M. Hedlund, T. Edvinsson, E.M.J. Johansson, G. Boschloo, H. Rensmo, T. Brinck, L. Sun, A. Hagfeldt, Rhodanine dyes for dye-sensitized solar cells: spectroscopy, energy levels and photovoltaic performance, Phys. Chem. Chem. Phys. 11 (2009) 133–141.

Please cite this article as: P. K. D. D. P. Pitigala, M. M. Henary and A. G. U. Perera, Effects of physical orientation of dye molecules and molecular orbitals on performance of solid-state dye sensitized solar cells, Materials Today: Proceedings, https://doi.org/10.1016/j.matpr.2019.06.189